Optics Letters

Chiral Zener tunneling in non-Hermitian frequency lattices

Lingzhi Zheng,[1] Bing Wang,[1,*] Chengzhi Qin,[1,3] Lange Zhao,[1] Shuyue Chen,[1] Weiwei Liu,[1] and Peixiang Lu[1,2]

[1]School of Physics and Wuhan National Laboratory for Optoelectronics, Huazhong University of Science and Technology, Wuhan, 430074, China
[2]Hubei Key laboratory of Optical Information and Pattern Recognition, Wuhan Institute of Technology, Wuhan, 430025, China
[3]e-mail: qinchengzhi@hust.edu.cn
*Corresponding author: wangbing@hust.edu.cn

Received 19 July 2022; revised 16 August 2022; accepted 17 August 2022; posted 18 August 2022; published 6 September 2022

A waveguide coupler under both phase and intensity modulation is proposed to generate a non-Hermitian Su–Schrieffer–Heeger lattice in frequency dimension. By varying the modulation period and phase, we can manipulate the on-site potential of the lattice and realize anisotropic coupling of the supermodes in waveguides. The artificial electric field associated with the modulation phase can also be introduced simultaneously. Zener tunneling is demonstrated in the non-Hermitian system and manifests an irreversibly unidirectional conversion between odd and even supermodes. The conversion efficiency can be optimized by varying the on-site potential of the waveguides. The study provides a versatile platform to explore non-Hermitian multiband physics in synthetic dimensions, which may find great application in chiral mode converters and couplers.

https://doi.org/10.1364/OL.470880

Zener tunneling (ZT) refers to the interband transition of electrons in solids with multiple energy bands as they are exposed to a high static electric filed [1]. The effect has been extended to optical [2], acoustic [3], and cold atom systems [4] and has spurred many interesting theoretical and experimental investigations. For example, ZT has been experimentally observed in two-dimensional photonic lattices [5]. Most previous works concerning ZT focus on the nonadiabatic evolution in Hermitian systems. Moreover, extensive research encompassing parity-time symmetry [6], non-Bloch-band theory [7], and topological phase in non-Hermitian systems [8] has been conducted to date. A recent study reveals that the ZT induced by resonant electric field forcing turns out to be chiral in the anisotropic Su–Schrieffer–Heeger (SSH) model [9]. The tunneling process is unidirectional and irreversible in non-Hermitian systems due to the existence of Floquet exceptional points (EPs) [10]. This feature is thoroughly different from that in Hermitian systems, where periodic oscillations are observable [11]. In order to implement such a theoretical model in real practice, it is challenging to construct a compact system furnishing multiple energy bands and anisotropic coupling. Although an optical configuration of coupled ring resonators may meet most of the requirements, the fabrication is demanding and the size is relatively massive [12,13].

In this work, we suggest that synthetic frequency dimension is capable of demonstrating non-Hermitian chiral ZT. The modes in an optical waveguide with evenly spaced frequencies couple to each other by applying dynamic refractive index modulation, forming a frequency lattice with tunable coupling strength and artificial gauge potential [14–16]. The synthetic frequency dimension makes it possible to generate a higher-dimensional lattice in lower-dimensional physical structures, and the non-Hermitian component is easily implemented. A number of intriguing physical phenomena have been demonstrated in synthetic dimensions, such as the quantum Hall effect [17], higher-order topological insulators [18], Weyl semimetals [19], the non-Hermitian skin effect [20–24], and non-Hermitian Bloch oscillations [25].

We demonstrate that coupled waveguides under complex refractive index modulation are able to generate a non-Hermitian SSH model in frequency dimension. Furthermore, by presetting the modulation wavenumber and initial phase, anisotropic coupling, on-site potential, and artificial electric field can be introduced to this two-band frequency lattice simultaneously. The non-Hermitian chiral ZT in the coupled waveguides is accompanied by irreversibly unidirectional mode conversion. The study provides a versatile platform to explore non-Hermitian multiband physics in synthetic dimensions and may find applications in spectrum manipulation and chiral mode converters.

We start by considering a pair of coupled waveguides undergoing dynamic index modulation as shown schematically in Fig. 1(a). The binary traveling-wave complex index modulations, as depicted in Figs. 1(b) and 1(c), have a phase difference of π between left and right waveguides as

$$\begin{aligned} n_L(z,t) &= -n_R(z,t) \\ &= dn_1\cos(\Omega_1 t - q_1 z + \varphi_1) + idn'_1\cos(\Omega_1 t - q_1 z + \varphi'_1) \\ &+ dn_2\cos(\Omega_2 t - q_2 z + \varphi_2) + idn'_2\cos(\Omega_2 t - q_2 z + \varphi'_2), \end{aligned} \tag{1}$$

where $n_{L(R)}$ is the refractive index modulation applied on the left (right) waveguide, $\Omega_{1,2}$ and $q_{1,2}$ are the common modulation frequency and wavenumber of real and imaginary refractive index modulations, and $dn_{1,2}$, $dn'_{1,2}$ and $\varphi_{1,2}$, $\varphi'_{1,2}$ are their respective

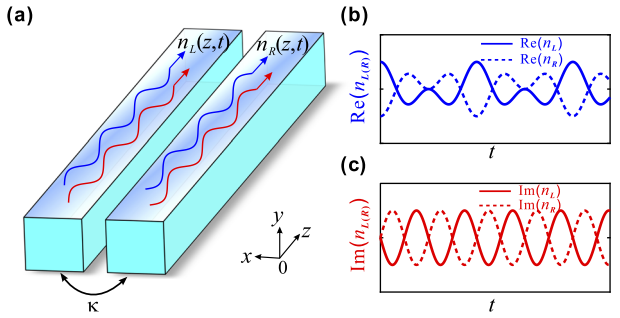

Fig. 1. (a) Coupled waveguides under complex dynamic refractive index modulation. The spatial coupling strength is denoted by κ. (b) Real and (c) imaginary parts of complex dynamic refractive index modulation of left and right waveguides. There is a phase difference of π in modulation between left and right waveguides, i.e., $n_L = -n_R$.

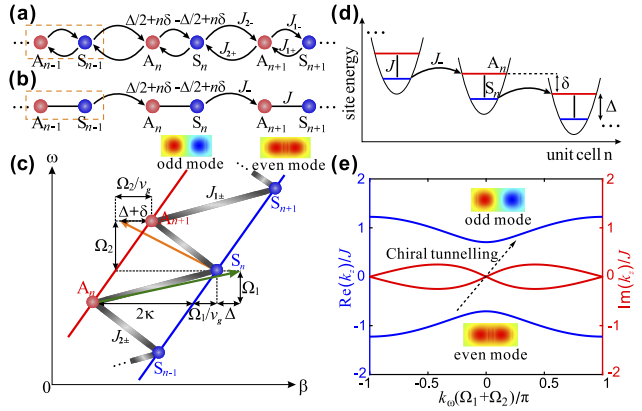

Fig. 2. (a) Equivalent general non-Hermitian SSH lattices. (b) Non-Hermitian SSH lattice with unidirectional intercell coupling. (c) Dispersion relation of coupled waveguides. (d) Distribution of on-site potential of non-Hermitian SSH lattice. The y axis represents the on-site potential of every site. (e) Chiral ZT between the two Bloch bands.

modulation amplitudes and initial phases. The physical implementation can be based on periodic modulation electrodes [25], placing p–n junction electrical diodes inside a slotted waveguide [26], and corrugated grating waveguide structure [27]. By applying dynamic index modulation, the supermodes with staggered frequencies are coupled to form an anisotropic SSH model, as shown in Fig. 2(a). Under specific modulation strength and initial phase, the coupled waveguide system can also mimic the SSH model with unidirectional intercell coupling as illustrated in Fig. 2(b), in which chiral ZT will occur. For concreteness, the evanescent coupling between the fundamental modes in each waveguide gives rise to the even and odd supermodes, forming a two-branch band, as shown in Fig. 2(c). The two branches are separated by a wavenumber difference 2κ, where κ denotes the coupling strength between the two waveguides. Then, a SSH lattice can be constructed by introducing interleaved mode transitions between the even and odd supermode bands. The modulation initial phase difference π between left and right waveguides is introduced due to the opposite parity between the even and odd supermodes. Using one modulation tone can introduce an interband transition between only two frequency modes [28]. On the contrary, two modulation tones can couple a series of supermodes and form frequency lattices. To satisfy the wavenumber matching condition as implied in the geometry of Fig. 2(c), and introduce staggered on-site potential and artificial dc electric field, the modulation wavenumbers are designed as

$$\begin{cases} q_1 = \Omega_1/v_g + 2\kappa + \Delta \\ q_2 = \Omega_2/v_g - 2\kappa - \Delta - \delta. \end{cases} \tag{2}$$

Due to the applied dynamic modulation with multiple frequencies $\Omega_{1,2}$, the electric field in the coupled waveguides can be expressed as

$$E(z,t) = \sum_{n,m} [a_{n,m}(z)\psi_L(x,y) + b_{n,m}(z)\psi_R(x,y)] \exp[i(\omega_{n,m}t - \beta_{n,m}z)], \tag{3}$$

where $a_{n,m}$ and $b_{n,m}$ are mode amplitudes of left and right waveguide with frequency $\omega_{n,m} = \omega_0 + n\Omega_1 + m\Omega_2$ and accompanying wavenumber $\beta_{n,m} = \beta_0 + n\Omega_1/v_g + m\Omega_2/v_g$, ($n$, $m = 0, \pm1, \pm2, \ldots$), v_g is the group velocity of the waveguide mode at ω_0, and $\psi_{L(R)}$ is the eigenmode profile of the isolated left (right) waveguide. The slight distinction of eigenmode profile between different frequencies and group velocity dispersion can be neglected under low-frequency modulation $\Omega_{1,2} << \omega_0$ [16]. Combining the coupled-mode equations in spatial and frequency dimensions [16], the whole coupled-mode equation is derived as

$$\begin{aligned} i\frac{d}{dz}\begin{bmatrix} a_{n,m} \\ b_{n,m} \end{bmatrix} &= \begin{bmatrix} 0 & \kappa \\ \kappa & 0 \end{bmatrix}\begin{bmatrix} a_{n,m} \\ b_{n,m} \end{bmatrix} \\ &+ J_{1+}e^{i(2\kappa z+\Delta z)}\begin{bmatrix} 1 & 0 \\ 0 & -1 \end{bmatrix}\begin{bmatrix} a_{n+1,m} \\ b_{n+1,m} \end{bmatrix} + J_{1-}e^{-i(2\kappa z+\Delta z)}\begin{bmatrix} 1 & 0 \\ 0 & -1 \end{bmatrix}\begin{bmatrix} a_{n-1,m} \\ b_{n-1,m} \end{bmatrix} \\ &+ J_{2+}e^{-i(2\kappa z+\Delta z+\delta z)}\begin{bmatrix} 1 & 0 \\ 0 & -1 \end{bmatrix}\begin{bmatrix} a_{n,m+1} \\ b_{n,m+1} \end{bmatrix} + J_{2-}e^{i(2\kappa z+\Delta z+\delta z)}\begin{bmatrix} 1 & 0 \\ 0 & -1 \end{bmatrix}\begin{bmatrix} a_{n,m-1} \\ b_{n,m-1} \end{bmatrix}. \end{aligned} \tag{4}$$

Transforming to supermode basis in a rotating frame and implementing the rotating wave approximation by omitting the large mismatching terms as $\exp(\pm 4i\kappa z)$ provided $\kappa >> \Delta$, δ, $|J_{1(2)\pm}|$, the coupled-mode equation describing the dynamic of supermodes is obtained:

$$\begin{cases} i\dfrac{d}{dz}A_n = \left(\dfrac{\Delta}{2} + n\delta\right)A_n + J_{1+}S_n + J_{2-}S_{n-1} \\ i\dfrac{d}{dz}S_n = \left(-\dfrac{\Delta}{2} + n\delta\right)S_n + J_{1-}A_n + J_{2+}A_{n+1}, \end{cases} \tag{5}$$

where A_n and S_n denote the electric field amplitude of odd mode with frequency $\omega_0 + (n-1)\Omega_1 + n\Omega_2$ and even mode with frequency $\omega_0 + n\Omega_1 + n\Omega_2$. The coupling coefficients are given by (see the Appendix of Ref. [25])

$$J_{1(2)\pm} = (dn_{1(2)}e^{\mp i\varphi_{1(2)}} + idn'_{1(2)}e^{\mp i\varphi'_{1(2)}})\omega_0/2c, \tag{6}$$

with c being the speed of light. Equation (5) indicates that the supermodes with staggered frequency sites are coupled by the dynamic modulation to form the SSH lattice as shown in Fig. 2(a). The wavenumber mismatching Δ and δ behave as the staggered on-site potential and artificial dc electric field on the frequency lattice.

To demonstrate the chiral ZT, the unidirectional intercell coupling should be achieved as $J_{2+} = 0$, and the intracell coupling can be isotropic as $J_{1+} = J_{1-}$, as shown in Fig. 2(b). This implies $dn'_1 = \varphi_1 = \varphi_2 = 0$, $\varphi'_2 = -\pi/2$, and $dn_2 = dn'_2$. The corresponding coupled-mode equation is obtained by Eqs. (5) and (6)

as

$$\begin{cases} i\dfrac{d}{dz}A_n = \left(\dfrac{\Delta}{2} + n\delta\right)A_n + JS_n + J_-S_{n-1} \\ i\dfrac{d}{dz}S_n = \left(-\dfrac{\Delta}{2} + n\delta\right)S_n + JA_n, \end{cases} \tag{7}$$

where $J = \omega_0 dn_1/2c$ and $J_- = \omega_0 dn_2/c$. The distribution of on-site potential of this non-Hermitian SSH lattice is illustrated in Fig. 2(d). Doing gauge transformation $A'_n(S'_n) = \exp(i\delta nz)A_n(S_n)$ and then going to k-space $A'_n(S'_n) = \int_{BZ} dk_\omega A_{k\omega}(S_{k\omega})\exp[-ik_\omega n(\Omega_1 + \Omega_2)]$, the coupled-mode equation for Bloch state $A_{k\omega=0}$ and $S_{k\omega=0}$ reads

$$i\frac{d}{dz}\begin{bmatrix} A_{k_\omega=0} \\ S_{k_\omega=0} \end{bmatrix} = \left\{\begin{bmatrix} \Delta/2 & J \\ J & -\Delta/2 \end{bmatrix} + \begin{bmatrix} 0 & J_-\exp(i\delta z) \\ 0 & 0 \end{bmatrix}\right\}\begin{bmatrix} A_{k_\omega=0} \\ S_{k_\omega=0} \end{bmatrix}, \tag{8}$$

where k_ω denotes the Bloch wave vector. Defining

$$\begin{aligned} H(z) &= H_0 + H'\exp(i\delta z), \\ H_0 &= \begin{bmatrix} \Delta/2 & J \\ J & -\Delta/2 \end{bmatrix},\ H' = \begin{bmatrix} 0 & J_- \\ 0 & 0 \end{bmatrix}, \end{aligned} \tag{9}$$

following the recent work of Stefano Longhi [9,10,29], as a non-Hermitian periodic Hamiltonian $H(z)$ is composed of a static part with real eigenvalues, e.g., H_0 with eigenvalues $\{E_0 = (\Delta^2/4 + J^2)^{1/2}, -E_0\}$, and a periodic part with solely positive or negative frequency component, e.g., $H'\exp(i\delta z)$, when δ satisfies resonant condition $|n\delta| = |2E_0|$, $(n = 1, 2, \ldots)$, a Floquet EP occurs. The two quasi-energies and corresponding Floquet eigenstates of a time-periodic non-Hermitian Hamiltonian both collapse. Therefore, there is a dominant state in the two instantaneous eigenstates of $H(z)$ depending on the sign of resonant forcing δ. After a long-distance evolution, the output light field will be mainly composed of the dominant state regardless of the excitation condition. Typically, for positive (negative) driven frequency δ, the dominant state will be the lower (higher) band Bloch eigenstate. It is worth noting that we introduce a large staggered on-site potential Δ to make the two Bloch eigenstates mainly consist of sublattice A (odd modes) and S (even mode) separately. The lattice model of non-Hermitian SSH model with unidirectional intercell coupling and the corresponding energy band are illustrated in Figs. 2(d) and 2(e). With the drift of Bloch wave vector to cyclically span the Brilliouin zone induced by artificial dc electric field, the chiral ZT between two Bloch bands occurs as shown in Fig. 2(e). The unidirectional intercell coupling, leading to the solely positive or negative frequency component in the periodic part of Eq. (8), is crucial to achieve this chiral dynamic.

We simulated the non-Hermitian chiral ZT in coupled waveguides under complex dynamic modulation by first-principles simulations using the finite-difference time-domain (FDTD) method and by solving the coupled-mode Eq. (7), as shown in Fig. 3. The input even mode frequency comb is Gaussian in frequency domain as

$$E(z = 0, x, t) = \psi_s(x)\sum_n e^{-n^2/D^2}e^{i(\omega_0 + n\Omega_1 + n\Omega_2)t}, \tag{10}$$

and the input odd mode frequency comb is

$$E(z = 0, x, t) = \psi_A(x)\sum_n e^{-n^2/D^2}e^{i[\omega_0 + (n-1)\Omega_1 + n\Omega_2]t}, \tag{11}$$

where $\psi_{S(A)}$ represents the even (odd) mode profile of coupled waveguides and D denotes the Gaussian width ($D = 4$ in

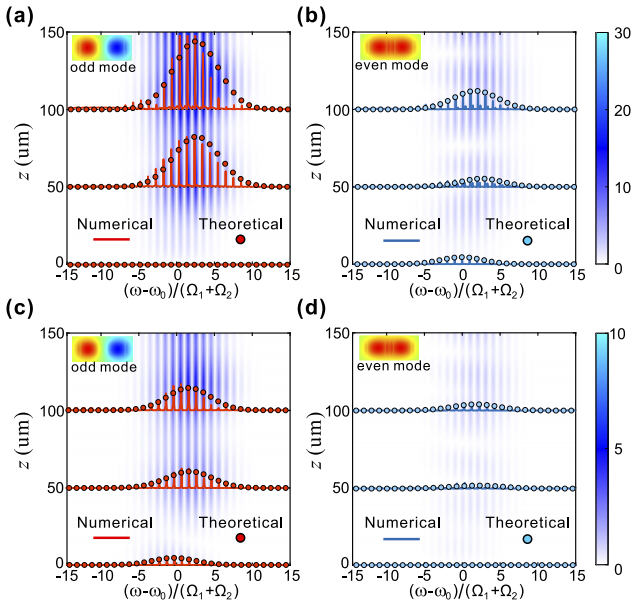

Fig. 3. Dynamic evolution of ZT under resonant forcing $\delta = -E_0$. (a), (b) Spectrum of odd and even modes with even mode excitation. (c), (d) Spectrum of odd and even modes with odd mode excitation. The blue (red) lines are the even (odd) mode spectra solved by the FDTD method, and filled circles are solved by coupled-mode Eq. (8).

Fig. 3). Equations (10) and (11) can be regarded as a Bloch wave packet of sublattice S and A with central Bloch vector $k_\omega = 0$, respectively. The supermode frequency comb can be excited by using an asymmetric directional coupler from different ports [27,30]. The system consists of two 400 nm width waveguides with 100 nm gap and static refractive index $n_0 = 2$ placed in air. The modulation parameters are $f_1 = \Omega_1/2\pi = 0.5$ THz, $f_2 = \Omega_2/2\pi = 1$ THz, $dn_1 = 0.02$, $dn_2 = dn'_2 = 0.05$, $\varphi'_2 = -\pi/2$, $\Delta = 0.2\ \mu m^{-1}$, and $dn'_1 = \varphi_1 = \varphi_2 = 0$. The central frequency is 1550 nm. As shown in Figs. 3(a) and 3(b), the input even modes are converted to odd modes accompanied by irreversible mode amplification and blueshift which indicates the chiral ZT process as shown in Fig. 2(e). Besides, with odd mode excitation, the output electric field is still mainly composed of odd modes as shown in Figs. 3(c) and 3(d). The first-principles simulated and theoretical spectra agree well with each other. To show the difference of ZT between resonant and nonresonant forcing, the evolution of light intensity of even and odd modes is depicted in Fig. 4. For resonant forcing, the ZT process is irreversible with mode amplification from even modes to odd modes, as shown in Figs. 4(a) and 4(b). On the contrary, for nonresonant forcing, the ZT becomes reversible as shown in Figs. 4(c) and 4(d). The algebraic secular growth of amplitude is a typical signature of a Floquet EP [10]. The Bloch states generally consist of both odd and even modes which hinders the mode conversion. Introducing staggered on-site potential Δ can decouple the sublattices in Bloch states and improve the mode conversion efficiency. As shown in Fig. 5(a), for lower staggered on-site potential $\Delta = 0$, the odd mode is less dominant in the output light field compared with the case for larger staggered on-site potential $\Delta = 0.4$ under even mode excitation. The proportion of odd modes in the output light field increases with the growth of staggered on-site potential, as shown in Fig. 5(b). The situation for odd mode excitation

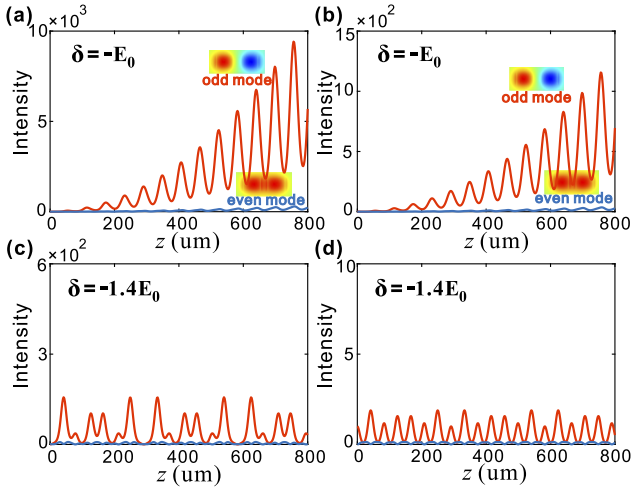

Fig. 4. Evolution of light intensity of odd and even modes under resonant forcing $\delta = -E_0$ with (a) even mode excitation and (b) odd mode excitation, and nonresonant forcing $\delta = -1.4E_0$ with (c) even mode excitation and (d) odd mode excitation.

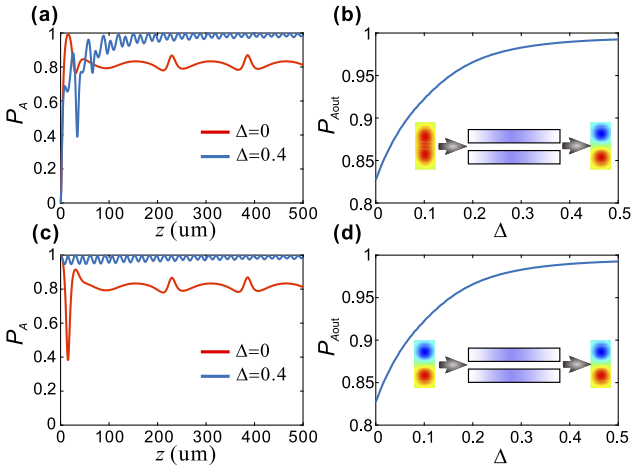

Fig. 5. Evolution of normalized light intensity of odd mode $P_A = I_A/(I_A + I_S)$ under (a) even mode excitation and (c) odd mode excitation. Output normalized light intensity of odd mode versus staggered on-site potential Δ under (b) even mode excitation and (d) odd mode excitation with 2 cm propagation distance.

is similar as shown in Figs. 5(c) and 5(d), which manifests the chiral behavior of the non-Hermitian ZT.

In summary, we construct a non-Hermitian SSH model in frequency dimension based on coupled waveguides under both phase and intensity modulation. Tunable anisotropy coupling, on-site potential, and artificial electric field can be introduced simultaneously. Furthermore, we simulate the non-Hermitian chiral ZT processes in our coupled waveguide system which manifests an irreversible unidirectional conversion between the odd and even supermodes. Varying the on-site potential of the waveguides can improve the conversion efficiency. Our system provides a versatile platform for demonstrating physical phenomena of non-Hermitian lattices in synthetic dimensions and has potential application in chiral mode converters and couplers.

Funding. National Natural Science Foundation of China (11974124, 12021004, 12147151).

Disclosures. The authors declare no conflicts of interest.

Data availability. Data underlying the results presented in this paper are not publicly available at this time but may be obtained from the authors upon reasonable request.

REFERENCES

1. C. Zener, Proc. R. Soc. A **145**, 523 (1934).
2. M. Ghulinyan, C. J. Oton, Z. Gaburro, L. Pavesi, C. Toninelli, and D. S. Wiersma, Phys. Rev. Lett. **94**, 127401 (2005).
3. H. Sanchis-Alepuz, Y. A. Kosevich, and J. Sánchez-Dehesa, Phys. Rev. Lett. **98**, 134301 (2007).
4. A. Zenesini, H. Lignier, G. Tayebirad, J. Radogostowicz, D. Ciampini, R. Mannella, S. Wimberger, O. Morsch, and E. Arimondo, Phys. Rev. Lett. **103**, 090403 (2009).
5. H. Trompeter, W. Krolikowski, D. N. Neshev, A. S. Desyatnikov, A. A. Sukhorukov, Y. S. Kivshar, T. Pertsch, U. Peschel, and F. Lederer, Phys. Rev. Lett. **96**, 053903 (2006).
6. C. M. Bender and S. Boettcher, Phys. Rev. Lett. **80**, 5243 (1998).
7. S. Yao and Z. Wang, Phys. Rev. Lett. **121**, 086803 (2018).
8. E. J. Bergholtz, J. C. Budich, and F. K. Kunst, Rev. Mod. Phys. **93**, 015005 (2021).
9. S. Longhi, Phys. Rev. Lett. **124**, 066602 (2020).
10. S. Longhi, J. Phys. A: Math. Theor. **50**, 505201 (2017).
11. S. Longhi, Europhys. Lett. **76**, 416 (2006).
12. X. Zhu, H. Wang, S. K. Gupta, H. Zhang, B. Xie, M. Lu, and Y. Chen, Phys. Rev. Res. **2**, 013280 (2020).
13. Z. Lin, L. Ding, S. Ke, and X. Li, Opt. Lett. **46**, 3512 (2021).
14. B. A. Bell, K. Wang, A. S. Solntsev, D. N. Neshev, A. A. Sukhorukov, and B. J. Eggleton, Optica **4**, 1433 (2017).
15. L. Yuan, Q. Lin, M. Xiao, and S. Fan, Optica **5**, 1396 (2018).
16. C. Qin, F. Zhou, Y. Peng, D. Sounas, X. Zhu, B. Wang, J. Dong, X. Zhang, A. Alu, and P. Lu, Phys. Rev. Lett. **120**, 133901 (2018).
17. L. Yuan, Y. Shi, and S. Fan, Opt. Lett. **41**, 741 (2016).
18. A. Dutt, M. Minkov, I. A. D. Williamson, and S. Fan, Light: Sci. Appl. **9**, 131 (2020).
19. Q. Lin, M. Xiao, L. Yuan, and S. Fan, Nat. Commun. **7**, 13731 (2016).
20. Y. Song, W. Liu, L. Zheng, Y. Zhang, B. Wang, and P. Lu, Phys. Rev. Appl. **14**, 064076 (2020).
21. S. Weidemann, M. Kremer, T. Helbig, T. Hofmann, A. Stegmaier, M. Greiter, R. Thomale, and A. Szameit, Science **368**, 311 (2020).
22. K. Wang, A. Dutt, K. Y. Yang, C. C. Wojcik, J. Vučković, and S. Fan, Science **371**, 1240 (2021).
23. K. Wang, A. Dutt, C. C. Wojcik, and S. Fan, Nature **598**, 59 (2021).
24. Y. Song, Y. Chen, W. Xiong, and M. Wang, Opt. Lett. **47**, 1646 (2022).
25. C. Qin, B. Wang, Z. J. Wong, S. Longhi, and P. Lu, Phys. Rev. B **101**, 064303 (2020).
26. H. Lira, Z. Yu, S. Fan, and M. Lipson, Phys. Rev. Lett. **109**, 033901 (2012).
27. Q. Liu, S. Li, B. Wang, S. Ke, C. Qin, K. Wang, W. Liu, D. Gao, P. Berini, and P. Lu, Phys. Rev. Lett. **124**, 153903 (2020).
28. Z. Yu and S. Fan, Nat. Photonics **3**, 91 (2009).
29. S. Longhi and G. Della Valle, Ann. Phys. **385**, 744 (2017).
30. C. Li, D. Liu, and D. Dai, Nanophotonics **8**, 227 (2018).